EBioMedicine 36 (2018) 347–357

Contents lists available at ScienceDirect

EBioMedicine

journal homepage: www.ebiomedicine.com

EBioMedicine
Published by THE LANCET

SIRT5 deacylates metabolism-related proteins and attenuates hepatic steatosis in ob/ob mice

Yipeng Du [a,*,1], Hao Hu [a,e,1], Saisi Qu [b,1], Jifeng Wang [c,1], Chaoju Hua [a,e], Jialing Zhang [a,e], Peng Wei [a,e], Xiaolong He [a,e], Junfeng Hao [f], Pingsheng Liu [a], Fuquan Yang [c], Tingting Li [b,d,*], Taotao Wei [a,*,2]

[a] National Laboratory of Biomacromolecules, Institute of Biophysics, Cthe Strategic Priority Research Programses, Beijing 100101, China
[b] Department of Biomedical Informatics, School of Basic Medical Sciences, Peking University Health Science Center, Beijing 100191, China
[c] Laboratory of Protein and Peptide Pharmaceuticals, Laboratory of Proteomics, Institute of Biophysics, Chinese Academy of Sciences, Beijing 100101, China
[d] Institute of Systems Biomedicine, School of Basic Medical Sciences, Peking University Health Science Center, Beijing 100191, China
[e] University of Chinese Academy of Sciences, Beijing 100049, China
[f] Core Facility for Protein Research, Institute of Biophysics, Chinese Academy of Sciences, Beijing 100101, China

ARTICLE INFO

Article history:
Received 22 June 2018
Received in revised form 18 September 2018
Accepted 19 September 2018
Available online 29 September 2018

Keywords:
Sirtuins
SIRT5
Malonylation
Succinylation
Metabolism
Proteomics

ABSTRACT

Background: Sirtuin 5 (SIRT5) is a NAD^+-dependent lysine deacylase. The SIRT5 deficiency mouse model shows that it is dispensable for metabolic homeostasis under normal conditions. However, the biological role of SIRT5 and acylation in pathological states such as obesity and type 2 diabetes (T2D) remains elusive.
Methods: The hepatic SIRT5-overexpressing ob/ob mouse model (ob/ob-SIRT5 OE) was established by CRISPR/Cas9 gene editing tool Protein malonylation and succinylation lysine sites were identified by immunoprecipitation coupled lipid chromatography - tandem mass spectrometry (LC-MS/MS) methods.
Findings: The ob/ob-SIRT5 OE mice showed decreased malonylation and succinylation, improved cellular glycolysis, suppressed gluconeogenesis, enhanced fatty acid oxidation, and attenuated hepatic steatosis. A total of 955 malonylation sites on 434 proteins and 1377 succinylation sites on 429 proteins were identified and quantitated. Bioinformatics analysis revealed that malonylation was the major SIRT5 target in the glycolysis/gluconeogenesis pathway, whereas succinylation was the preferred SIRT5 target in the oxidative phosphorylation pathway.
Interpretation: Hepatic overexpression of SIRT5 ameliorated the metabolic abnormalities of ob/ob mice, probably through demalonylating and desuccinylating proteins in the main metabolic pathways. SIRT5 and related acylation might be potential targets for metabolic disorders.
Fund: National Key R&D Program of China, the National Natural Science Foundation of China, the Strategic Priority Research Programs (Category A) of the Chinese Academy of Sciences, the Interdisciplinary Medicine Seed Fund of Peking University and the National Laboratory of Biomacromolecules.

1. Introduction

Sirtuins are a family of conserved nicotinamide adenine dinucleotide (NAD)-dependent deacylases that play important roles in various physiological and pathological processes [1]. There are seven sirtuins (SIRT1-7) in mammalian cells. SIRT1 to SIRT3 exhibit the most deacetylation activity and target a variety of proteins involved in cellular metabolism and energy homeostasis [2,3]. SIRT4 has been reported as a deacylase, and plays an important role in leucine metabolism and insulin secretion [4]. SIRT6 possesses many enzymatic activities including ADP-ribosyltransferase [5], deacetylase [6], and long-chain deacylase [7,8]. Similar to SIRT6, SIRT7 hydrolyzes long-chain fatty acyl modifications but in an rRNA-dependent way [9]. In addition, SIRT7 is also a protein deacetylase and desuccinylase [10,11].

Unlike the aforementioned sirtuins, SIRT5 is unique for its robust lysine-demalonylase, -desuccinylase, and -deglutarylase activities [12–14]. Proteomic studies have identified thousands of malonylation, succinylation, and glutarylation lysine sites in both wild-type and SIRT5 KO mice [14–18]. Analyses of these acylation datasets demonstrated the enrichment of proteins in various metabolic pathways including glycolysis/gluconeogenesis, fatty acid β-oxidation, and oxidative phosphorylation. Many proteins in these metabolic pathways are targeted by SIRT5. Indeed, deficiency of SIRT5 in cells has been

* Corresponding authors.
E-mail addresses: duyipeng@ibp.ac.cn (Y. Du), litt@hsc.pku.edu.cn (T. Li), weitt@ibp.ac.cn (T. Wei).
[1] These authors are equal contributors.
[2] Lead contact.

https://doi.org/10.1016/j.ebiom.2018.09.037

Research in context

Evidence before the study

Evidences of the biological role of SIRT5 were mostly from studies of SIRT5 deficiency mouse models. Yu et al. observed little phenotype of SIRT5 deficiency mice under the basal high-fat diet (HFD) challenged conditions. Interestingly, Sadhukhan et al. and Hershberger et al. have demonstrated that SIRT5 is required for a normal cardiac function under the condition of aging or cardiac pressure overloading. At the molecular level, SIRT5 has been suggested to regulate biological processes of ammonia detoxification, glycolysis, fatty acid oxidation, and ketone body production. The studies were all done based on the mouse model of SIRT5 deficiency. Although Ogura et al. established SIRT5 Tg mice, they also generated it in the non-ob/ob mice.

Added value of this study

The current studies established SIRT5 overexpression mouse model on the basis of ob/ob mouse strain. The findings here provide evidences to evaluate the role of SIRT5 under pathological conditions.

Implications of all the available evidence

Summarizing all the available evidences about biological function SIRT5 from studies of both deficiency and overexpression, normal and obesity mouse models, it seems that SIRT5 do play an important role in key metabolic biological processes, but in a chronic and humble way. Thus, long term observation and high sensitive detection methods are suggested in experiments designed to further explore the role of SIRT5 in details.

shown to inhibit glycolysis, suppress fatty acid β-oxidation, and attenuate ketone body production through regulating levels of malonylation or succinylation on key enzymes such as GAPDH [18], VLCAD [17], and HMGCS2 [16]. Despite the well-studied biological roles of SIRT5 at molecular and cellular levels, SIRT5 seems to be dispensable for metabolic homeostasis in normal conditions at the whole animal level [19]. However, recent studies have revealed that SIRT5 protects mice from ischemia-reperfusion injury, cardiac dysfunction induced by aging and cardiac-pressure overload [20–22]. This protective role is mediated by desuccinylation of proteins in fatty acid oxidation and oxidative phosphorylation pathways. Considering its widespread expression and large number of substrates, SIRT5 can function in more pathological conditions, especially in chronic metabolic diseases such as obesity and type 2 diabetes (T2D).

Interestingly, proteomic hypermalonylation in ob/ob mice has been observed by our group and confirmed by Bowman et al. [23,24]. Consistent with this observation, malonyl-CoA, the group donor of malonylation, has been shown to elevate in the skeletal muscle and the liver of OLETF rats and in muscle biopsies of patients with obesity and T2D [25,26]. Because SIRT5 plays pivotal roles in metabolic regulation and is the sole enzyme that catalyzes the demalonylation reaction, we hypothesized that SIRT5 and its deacylase activity might play an important role in insulin resistance of obesity and T2D [27]. To address this hypothesis, we used the T2D ob/ob mouse model. An alternative *Sirt5* gene was introduced into the mouse genome and specifically overexpressed in liver. Hepatic overexpression of SIRT5 significantly reduced levels of protein malonylation and succinylation. A series of biochemical, cellular biological and whole-animal characterization analyses were carried out.

2. Materials and methods

2.1. Antibodies and reagents

Anti-acetyllysine (PTM-105), anti-malonyllysine (PTM-901), anti-succinyllysine (PTM-401), anti-glutaryllysine (PTM-1151), anti-succinyllysine conjugated agarose beads (PTM-402), and anti-malonyllysine conjugated agarose beads (PTM-904) were purchased from PTM Biolabs. SIRT5 (Cat# 15122-1-AP, RRID:AB_2188778), NDUFS4 (15849-1-AP), COXIV(Cat# 11242-1-AP, RRID:AB_2085278), and GAPDH (Cat# 60004-1-Ig, RRID:AB_2107436) antibodies were purchased from ProteinTech. ATP5A (Cat# ab14748, RRID:AB_301447), UQCRC2 (Cat# ab14745, RRID:AB_2213640), SDHB (Cat# ab14714, RRID:AB_301432) and COXII (Cat# ab110258, RRID:AB_10887758) were from Abcam. TOM20 (Cat# 612278, RRID:AB_399595) was from BD Biosciences. pCPT-cAMP (C3912-10MG), glucose detection kit (GAGO20-1KT), lactate detection kit (MAK064-1KT), β-hydroxybutyrate assay kit (MAK041) and free fatty acid quantitation kit (MAK044) were from SigmaAldrich. Neutral lipid probe LipidTOX (H34475) was from Invitrogen. Sequencing-grade trypsin (V5113) was purchased from Promega. A list of other chemicals used for lipid chromatography – tandem mass spectrometry (LC-MS/MS) can be found in a previous paper [23].

2.2. Animals and samples

The original Sirt5 conditional knock-in C57BL/6 mouse was generated by Biocytogen (Beijing, China). Briefly, the targeting vector was constructed by inserting *Sirt5* coding sequence into the pCAGGS vector which contains a CAG promoter, WPRE 3` UTR and Ploy A sequences. A floxed "Stop" elements were then inserted between CAG promoter and Sirt5 CDS region (Fig. S1A). After cloning the 5′ and 3′ homologous arms of the *Hipp 11* locus on chromosome 11 into the vector, the vector was linearized and micro-injected into the mouse fertilized eggs together with the mRNA of CRISPR/Cas9 system. *Hipp 11* locus has been shown to be a safe, intergenic and transcriptionally active region of chromosome 11, as the Rosa 26 locus [28]. Correct insertion was confirmed by Southern blot experiments (Fig. S1C). A total of 11 founders from C57BL/6 background have been identified and used for further breeding. To specifically overexpress Sirt5 gene in liver of ob/ob mouse, a sequential crossing procedure was done among homozygous Sirt5 KI mouse, heterozygous Alb-cre mouse and heterozygous ob/+ mouse (Fig. 1B). All the mice are under C57BL/6 background. Two strains of mice were obtained under the procedure. One was the Sirt5 hepatic overexpressing (ob/ob-SIRT5 OE) mouse containing at least one allele of alternative Sirt5 gene and Alb-cre. The other one was control ob/ob mouse (ob/ob-Control) containing only the floxed Sirt5 KI allele. Males of those two strains at the age of 5 to 7 months were used for the experiences in the current work. Mouse studies were approved by the Animal Experimentation Ethics Committee (Institute of Biophysics, CAS) and the National Health and Medical Research Council of China Guidelines on Animal Experimentation.

2.3. Genotyping of the Ctl and OE mouse

Genotype of the mouse was under the standard PCR procedure. Briefly, mice tails were incubated with lysis buffer (100 mM Tris-Cl pH 8·5, 300 mM NaCl, 0·5 mM EDTA, 0·5% SDS, 0·2 mg/mL Protease K and 0·5 mg/mL RNase A) overnight at 55 °C. DNA was extracted by phenol/chloroform/isoamyl alcohol buffer and washed twice by 70% ethanol and dissolved in TE buffer (10 mM Tris-Cl pH 8·0, 0·5 mM EDTA). Primers used for genotyping include Alb-creF: 5-GAAGCAGAA GCTTAGGAAGATGG-3, Alb-creR: TTGGCCCCTTACCATAACTG; Leptin-muF: 5-TGACCTGGAGAATCTCT-3, Leptin-muR: 5-CCTGAAGACCCCTG GAA-3; SIRT5 KIF: 5-AGTACCAGACTGCCCTGA-3, SIRT5KIR: 5-CACTCC CACTGTCCTTTC-3. Genotype were repeated before experiments.

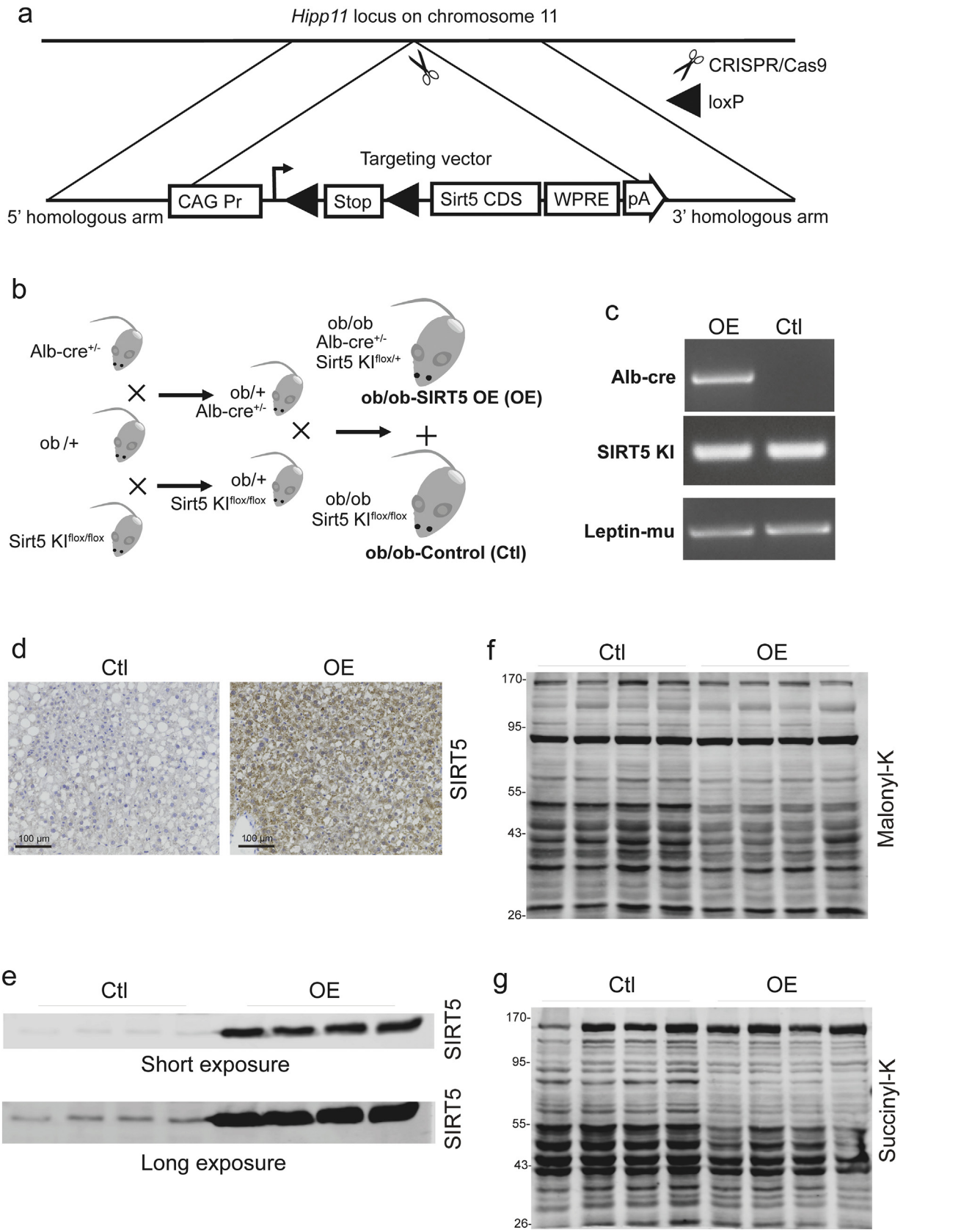

Fig. 1. Generation of ob/ob-SIRT5 OE mice. See also Fig. S1. (a) Strategy of an alternative *Sirt5* allele knock-in by CRISPR/Cas9 method. (b) Schematic diagram for breeding strategy to generate ob/ob-SIRT5 OE (OE) and ob/ob-Control mice (Ctl). (c) Examples of genotyping results. (d and e). Representative Immunohistochemistry (IHC) (d) and Western blot detection (e) of liver tissues from Ctl and OE mice determined with anti-SIRT5 antibody. (f and g) Western blot detection with pan anti- malonyllysine (f) and anti- succinyllysine (g) antibodies in the same samples as that of "e".

2.4. Primary hepatocyte isolation

Mice were anesthetized and abdominal cavity was dissected. The liver was perfused with KRG buffer (120 mM NaCl, 20 mM NaHCO3, 20 mM glucose, 5 mM HEPES pH 7·4, 5 mM KCl, 1 mM $MgSO_4$, 1 mM KH_2PO_4) with 0·5 mM EGTA through the visceral vena cava. Two minutes later, when the blood drains out, the solution is switched to KRG buffer with 25 mg/mL collagenase type 4. The liver is cut to release the hepatocytes. The hepatocytes are washed with ice-cold DMEM and the suspension passed through a 75 μm cell strainer, and spun at 50 *g* for 1 min. The wash step is repeated until the supernatant appear clear after spinning. The pellet was suspended with full culture medium and transferred to culture plates.

2.5. Glucose detection, intraperitoneal glucose tolerance test (ipGTT)

Serum glucose levels were detected by the Accu-Chek Blood Glucose Meter (Roche). Random glucose was detected at 11 am with normal diet. Fasting glucose was detected at 9 am after overnight fasting. Glucose levels of culture medium were detected by the Glucose Assay Kit (Sigma-Aldrich) following the manufacturer's instructions. For ipGTT, mice fasted 16 h. The baseline glucose levels ($t = 0$) were recorded using blood from the tip of mouse tail. 30 min later, glucose (2 g glucose/kg body weight) were injected. The blood glucose level was measured at 15, 30, 60, 90, 120, 180, and 240 min ($t = 15$, $t = 30$, $t = 60$, $t = 90$, $t = 120$, $t = 180$, and $t = 240$).

2.6. Body component detection and respiratory rate (RER) determination

Body components including fat mass and lean mass were detected by EchoMRI following the manufacture's instruction. VO_2, VCO_2, and RER were determined by the TSE Phenomaster System with the standard procedures. Mice were put into the cage 1 day before detection. Concentration of O_2, CO_2, and RER were detected and calculated every 6 min for 2 days. Five male mice per group were used in this experiment.

2.7. Soxhlet extraction of liver lipids

Whole livers were isolated and dried at 50 °C for 7 days. The dried livers were weighted and put into Soxhlet extraction apparatus with the solvent of diethyl ether. The extraction lasts for 4 h at the temperature of 35 °C. After extraction, livers were dried for an additional hour to get rid of the residual solvent. Then, livers were weighted again. Total lipids (mainly triglyceride, TG) in the liver were the weight difference before and after extraction.

2.8. Cellular fractionation, western blotting, coomassie blue staining, and immunofluorescence

Tissue subcellular fractionation was performed following standard protocols [29]. Western blotting and Coomassie blue staining analysis were carried out following protocols described previously [23]. Immunofluorescence and confocal microscopy was performed as previously described [30].

2.9. Pathway enrichment analysis

Biological pathway enrichment for malonylated and succinylated proteins was analyzed by DAVID Web Services (DAVID 6·8). All malonylated and succinylated proteins and SIRT5-regulated malonylation and succinylation proteins (Ctl/OE Ratio ≥ 2, *p*-value<0·05) were submitted. The whole mouse proteomic was used as background. The default parameters were used for our analysis. Fisher exact p-value was used to estimate the enrichment of pathways. All the enrichment pathways were summarized in Table S3. Enrichment of main metabolic pathways including "Fatty acid degradation", "Glycolysis / Gluconeogenesis", "TCA cycle", and "Oxidative phosphorylation" were selected and are shown in Fig. 2J and K.

2.10. Tissue lysate preparation, tryptic digestion and affinity enrichment of acylated peptides

Four mice per group were scarified by cervical dislocation. Tissues were homogenized in 1 mL lysis buffer (50 mM Tris-Cl pH 7·4, 150 mM NaCl, 0·5 mM EDTA, 1 mM dithiothreitol, 1% Triton X-100, 0·5% sodium deoxycholate, and 0·1% sodium dodecyl sulfate). The homogenized tissues were centrifuged at 12,000 rpm and the supernatant containing the tissue lysates were precipitated with acetone and resolved in 8 M urea with 50 mM Tris-HCl, pH 8·0. The samples were reduced by 10 mM dithiothreitol, alkylated by 10 mM iodoacetamide (45 min at RT in the dark), and digested with sequencing-grade modified trypsin (Promega) with a substrate ratio of 1:50 (w/w) overnight at 37 °C. After digestion, the samples were desalted and fractionated by eluting with different concentration of acetonitrile (from 5% to 80%). The fractionated peptides were dried and resolubilized in NETN buffer (50 mM Tris–Cl, pH 8·0, 0·5% NP-40, 100 mM NaCl, and 1 mM EDTA). Anti-malonyllysine antibody-conjugated resin was first added and incubated at 4 °C for 12 h with gentle shaking. Then the samples were centrifuged at the speed of 2000 *g* for 2 min. The supernatant was collected and anti-succinyllysine antibody-conjugated resin was added and incubated at 4 °C for 12 h with gentle shaking to precipitate succinyllysine peptides (Fig. 4A). Both anti-malonyllysine and anti-succinyllysine antibody-conjugated beads were washed two times with NETN buffer, once with ETN buffer (50 mM Tris–Cl, pH 8·0, 100 mM NaCl, and 1 mM EDTA) and once with purified water. The bound peptides were eluted by 0·1% trifluoroacetic acid and dried using the SpeedVac. The dried peptides were dissolved in 0·1% FA and desalted with C18 ZipTips.

2.11. Protein identification and quantification by LC-MS/MS

The nanoLC-MS/MS experiments were performed on a Q Exactive (Thermo Scientific) equipped with an Easy n-LC 1000 HPLC system (Thermo Scientific). The labeled peptides were loaded onto a 100 μm id×2 cm fused silica trap column packed in-house with reversed phase silica (Reprosil-Pur C18 AQ, 5 μm, Dr. Maisch GmbH) and then separated on an a 75 μm id×20 cm C18 column packed with reversed phase silica (Reprosil-Pur C18 AQ, 3 μm, Dr. Maisch GmbH). The peptides bounded on the column were eluted with a 135-min linear gradient. The solvent A consisted of 0·1% formic acid in water solution and the solvent B consisted of 0·1% formic acid in acetonitrile solution. The segmented gradient was 4–8% B, 5 min; 8–22% B, 90 min; 22–32% B, 22 min; 32–95% B, 3 min; 95% B, 15 min at a flow rate of 300 nL/min.

The MS analysis was performed with Q Exactive mass spectrometer (Thermo Scientific). With the data-dependent acquisition mode, the MS data were acquired at a high resolution 70,000 (m/z 200) across the mass range of 300–1600 m/z. The target value was 3·00E + 06 with a maximum injection time of 60 ms. The top 20 precursor ions were selected from each MS full scan with isolation width of 2 m/z for fragmentation in the HCD collision cell with normalized collision energy of 30%. Subsequently, MS/MS spectra were acquired at resolution 17,500 at m/z 200. The target value was 5·00E + 04 with a maximum injection time of 80 ms. The dynamic exclusion time was 40s. For nano electrospray ion source setting, the spray voltage was 2.0 kV; no sheath gas flow; the heated capillary temperature was 320 °C.

The raw data from Q Exactive were analyzed with Proteome Discovery version 2·2·0·388 using Mascot (version 2·5·1) and Sequest HT search engine for protein identification and Percolator for false discovery rate (FDR) analysis. The Uniprot mouse protein database (updated on 03-2017) was used for searching the data from mouse sample. Some important searching parameters were set as following: trypsin

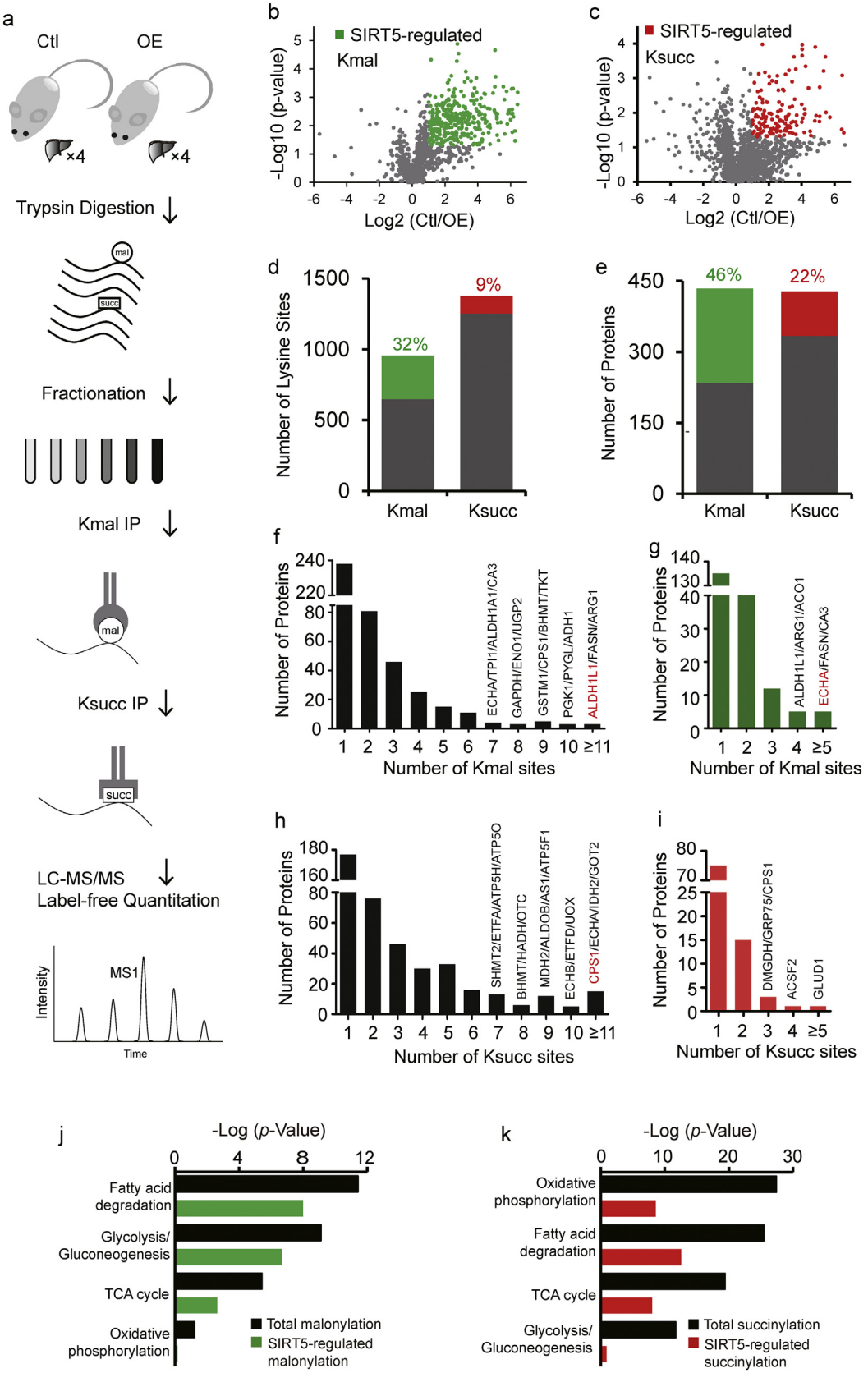

Fig. 2. Identification, quantification, and analysis of malonylome and succinylome. (a) Diagram of strategy for proteomic identification of malonylome and succinylome. (b and c) Fold change distribution of Kmal and Ksucc peptides between Ctl and OE samples. Green and red dots indicates SIRT5-regulated Kmal and Ksucc peptides with the threshold of ratio (Ctl/OE) ≥2 and p-value <0·05. (d and e) Number of Kmal and Ksucc sites (d) and proteins (e). Green and red column indicates number of SIRT5-regulated Kmal and Ksucc sites or proteins. (f and g) Distribution of number of total (f) and SIRT5-regulated (g) Kmal sites on proteins. Typical proteins with large number of modified lysine sites were listed. (h and i) Distribution of number of total (h) and SIRT5-regulated (i) Ksucc sites on proteins. Typical proteins with large number of modified lysine sites were listed. (j and k) Pathway enrichment of Kmal and Ksucc proteins. Four main metabolic pathways were selected to represent. Black column: total Kmal or Ksucc proteins. Green: SIRT5-regulated Kmal proteins. Red: SIRT5-regulated Ksucc proteins.

was selected as enzyme and two missed cleavages were allowed for searching; the mass tolerance of precursor was set as 10 ppm and the product ions tolerance was 0·02 Da.; the cysteine carbamidomethylation were specified as fixed modifications; The methionine oxidation and Lys malonylation (+86·0004 Da) or Lys succinylation (+100·0160 Da) were chosen as variable modifications. FDR analysis was performed with Percolator and FDR <1% was set for protein identification. The peptides confidence was set as high for peptides filter. Protein label-free quantification was also performed on Proteome Discovery 2·2·0·388 using the areas of identified peptides. Only unique and razor peptides of proteins were selected for protein relative quantification. The normalization to the protein median of each sample was used to correct experimental bias and the normalization mode was selected as total peptide amount. Protein ratios were calculated as median of all possible pairwise ratios. Missing values were imputed using low abundance resampling model.

3. Results

3.1. Generation of ob/ob-SIRT5 OE mice

An alternative SIRT5 coding sequence was inserted into the *Hipp 11* locus on chromosome 11 of wild-type C57BL/6 mice by the CRISPR/Cas9 method (Fig. 1a). The success of correct knock-in was confirmed and off-target insertion was excluded by Southern blot experiments (Fig. S1a–c). Hepatic SIRT5-overexpressing ob/ob mice (ob/ob-SIRT5 OE) and the control mice (ob/ob-Control) were generated by sequential crossing among the *Sirt5* allele knock-in mice (Sirt5 KI$^{flox/flox}$), Alb-cre mice (Alb-cre$^{+/-}$) and heterozygous ob/ob mice (ob/+) (Fig. 1b). Genotyping demonstrated that both ob/ob-SIRT5 OE (OE) and ob/ob-Control (Ctl) mice contained the alternative *Sirt5* allele, but only OE mice contained the Alb-cre allele (Fig. 1c). Consistent with the genotyping results, overexpression of SIRT5 in liver samples of OE mice was also confirmed by immunohistochemistry (Fig. 1d) and Western blot experiments (Fig. 1e). There was a great decrease of total protein malonylation and succinylation in liver tissues from OE mice compared to that of Ctl mice (Fig. 1f and g), whereas the total protein level and β-actin were comparable (Fig. S2h). Additionally, overexpression of SIRT5 was not observed in other tissues including white adipose tissue, heart, muscle, and spleen (Fig. S2a–d). Although there was a slight increase of SIRT5 in kidney of OE mice, levels of malonylation and succinylation in kidney were not significantly affected (Fig. S2f and g).

To detect the localization of overexpressed SIRT5 proteins, we performed the immunofluorescence experiments and found that signal of SIRT5 proteins merged well with that of mitochondrial biomarker protein TOM20 (Fig. S1d), suggesting the mitochondrial localization of SIRT5. Because previous work showed that endogenous SIRT5 proteins localized in both mitochondria and cytosol [15], we then further determined the localization of SIRT5 by cell fractionation and found that overexpressed SIRT5 proteins were also localized in the cytosol (Fig. S1e). Altogether, we overexpressed SIRT5 in liver of ob/ob mice, which significantly reduced levels of malonylation and succinylation on multiple proteins.

3.2. Identification, quantification, and analysis of the malonylome and succinylome in response to hepatic overexpression of SIRT5 in ob/ob mice

To identify the malonylome and succinylome in response to hepatic overexpression of SIRT5 in ob/ob mice, we developed a workflow involving enrichment of malonylated and succinylated peptides coupled with identification by tandem mass spectrometry (Fig. 2a). With this approach we identified and quantified 1100 unique peptides corresponding to 955 lysine sites on 434 proteins for malonylation and 1790 unique peptides corresponding to 1377 lysine sites on 429 proteins for succinylation with a FDR of <1% (Table S1). The peptides were quantitated by the PD2·4 Label-Free Quantitation Program which extracts and measures ion intensity chromatograms of MS1 scan. For each unique peptide, abundance ratios (Ctl/OE) and *p*-values were calculated between the four Ctl and four OE samples based on the quantification results. Levels of malonylation were down-regulated on 329 out of 1100 peptides with ratio (Ctl/OE) increase ≥2-fold and p-value <0·05 (Fig. 2b). This represented 306 out of 955 (32%) malonylated lysine (Kmal) sites and 200 out of 434 (46%) malonylated proteins (Fig. 2d and e). Meanwhile, levels of succinylation were down-regulated on 146 out of 1790 peptides by the same threshold (Fig. 2c), which corresponded to 123 out of 1377 (9%) succinylated lysine (Ksucc) sites, and 95 out of 429 (22%) succinylated proteins (Fig. 2d and e). Although the abundance of malonylation and succinylation changed greatly from Ctl to OE mice, the abundance of proteins was not significantly altered (Table S1), for 99% of proteins (3098/3145) changed less than one fold among the 3145 quantified proteins (Fig. S3a).

To analyze the distribution of malonylation and succinylation at protein level, we calculated the number of Kmal and Ksucc sites on each protein (Fig. 2f–i). The data showed that some proteins were intensively modified. For example, 35 unique peptides corresponding to 20 Kmal sites on ALDH1L1 were identified (Figs. 2f and S3b), and 63 unique peptides representing 36 Ksucc sites on CPS1 were found (Figs. 2h and S3c). There were also proteins highly regulated by SIRT5. For instance, all seven identified malonylation sites on ECHA were targeted by SIRT5 (Figs. 2g and S3d). Interestingly, Sadhukhan et al., recently reported that SIRT5 could regulate the activity of ECHA through desuccinylation [20]. They identified 28 succinylated lysine sites on ECHA, which was regulated by SIRT5. Six out of the seven malonylated lysine sites in this study were overlapped with the 28 succinylated lysine sites. These results suggested that demalonylation might be another mechanism that SIRT5 regulates the activity of ECHA. In addition, we compared the SIRT5-regulated malonylation dataset identified using hepatic SIRT5-overexpressing mice with a previous dataset identified using SIRT5-deficient mice [18]. We found that 32 lysine sites overlapped between 306 SIRT5-targeted sites in our overexpression dataset and 183 SIRT5-regulated sites in the deficiency dataset (Table S2, Fig. S3e and f). We propose that these 32 lysine sites across 25 proteins were the most potential SIRT5-mediated demalonylation substrate sites. We also compared the malonylome and succinylome and found limited overlap between the two types of acylation (Fig. S4a and b). Most of the highly malonylated proteins (≥10 Kmal sites per protein) were slightly succinylated, whereas most of the heavily succinylated proteins (≥10 Ksucc sites per protein) were moderately malonylated (Fig. S4c). Interestingly, all the highly malonylated proteins were localized in the cytosol, whereas almost all the heavily succinylated proteins were in mitochondria (Fig. S4c). These results suggest that the malonylome is significantly distinct from the succinylome.

3.3. Hepatic overexpression of SIRT5 in ob/ob mice demalonylates proteins in the glycolysis/gluconeogenesis pathway to improve glucose metabolism, and desuccinylates proteins in the oxidative phosphorylation pathway to facilitate fatty acid metabolism

To investigate the potential pathways regulated by SIRT5, pathway enrichment analysis was done using DAVID Web Services (Table S3) [31]. For those SIRT5-regulated proteins, there was little enrichment for malonylated proteins on “Oxidative phosphorylation” pathway (Figs. 2j and 3g), and reduced enrichment for succinylated proteins on the “Glycolysis/Gluconeogenesis” pathway (Figs. 2k and 3a).

To determine whether the Glycolysis/Gluconeogenesis pathway was authentically affected by SIRT5 overexpression, lactic acid was detected in the medium of hepatocytes derived from Ctl and OE mice. We found that the level of lactic acid in OE hepatocytes were higher than that of Ctl hepatocytes (Fig. 3b). To confirm the result, extracellular acidification (ECAR) value was examined when glucose was provided as the only source for energy metabolism. We found that ECAR value in OE

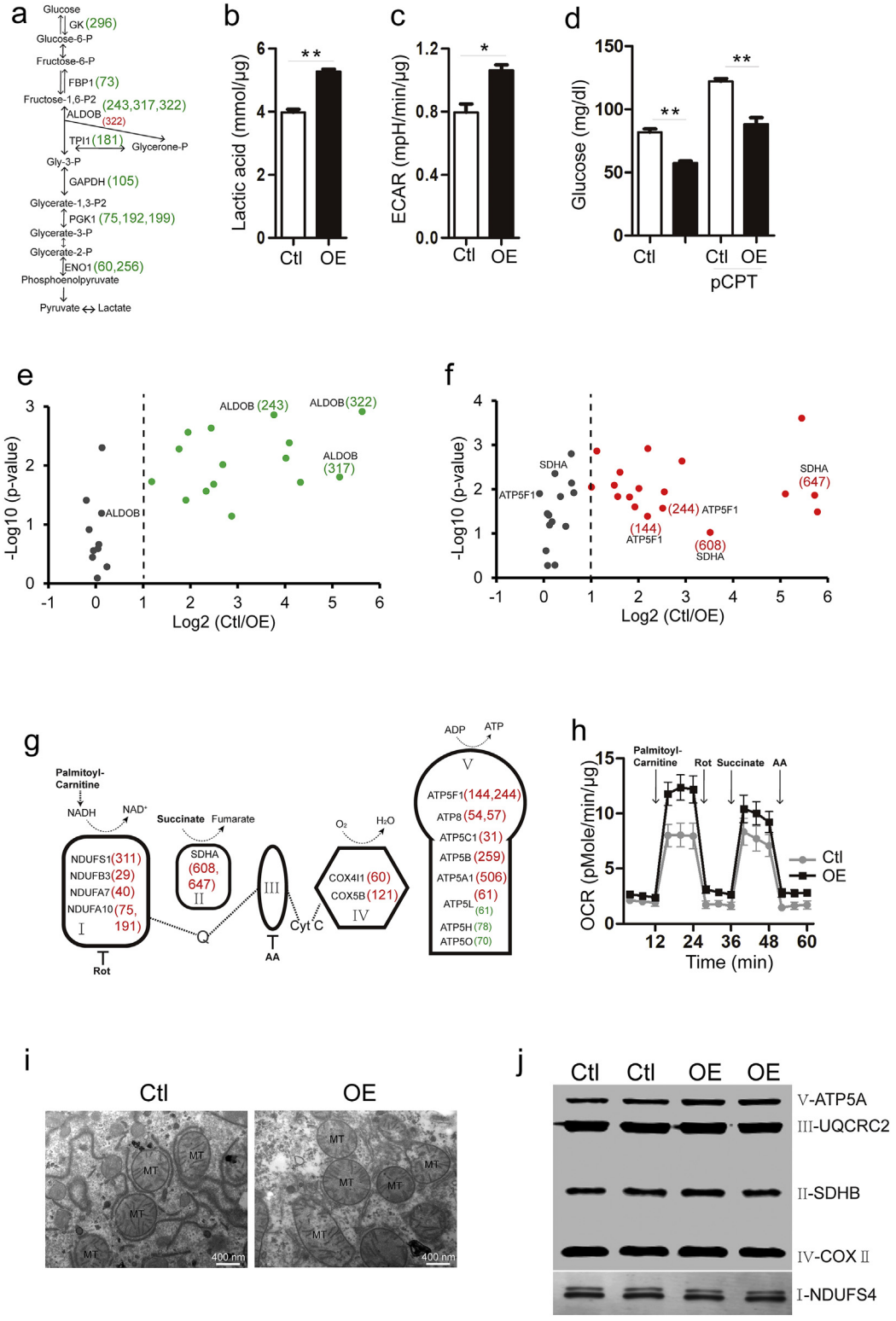

Fig. 3. Hepatic overexpression of SIRT5 in ob/ob mice demalonylates proteins in the Glycolysis / Gluconeogenesis pathway to improve glucose metabolism, and desuccinylates proteins in the oxidative phosphorylation pathway to facilitate fatty acid metabolism. (a) Proteins and acylation sites regulated by SIRT5 overexpression in glycolysis pathway. Red: Ksucc sites; Green: Kmal sites. (b) Levels of lactic acid in culture medium of primary hepatocytes 24 h after isolation. Data are represented as mean ± SEM. N = 3; **: P < 0·01. (c) Extracellular acidification rate (ECAR) of primary hepatocytes 24 h after isolation. Glucose were provide as the only carbon source. N = 3; *: P < 0·05. (d) Levels of glucose in culture medium of primary hepatocytes after 6 h incubating with glucose-free medium containing lactate, pyruvate and glutamine. pCPT: pCPT-cAMP is an PKA activator which promote gluconeogenesis. N = 6. (e and f) Fold change (Ctl/OE) of Kmal sites (Green), Ksucc sites (Red) and expression levels of related proteins (Gray) in glycolysis (e) and oxidative phosphorylation pathways (f). Several represent sites and proteins were marked. (g) Proteins and acylation sites regulated by SIRT5 overexpression in oxidative phosphorylation pathway. Red: Ksucc sites; Green: Kmal sites. (h) Oxygen consumption rate (OCR) detection of primary hepatocytes from Ctl and OE mice. Palmitoyl-cartinine or Succinate were used as substrates. Rot: rotenone; AA: antimycin A. Error bars were calculated based on 10 technical repeats for each pair of Ctl and OE mice. A total of 3 pairs of Ctl and OE mice were detected. One pair of representative results was present here. (i) Electron microscope observation of liver tissues from Ctl and OE mice with magnification of 30,000×. MT: mitochondria.
(j) Western blot detection of five represent proteins from five complex (I-V) in oxidative phosphorylation pathway.

hepatocytes was also higher than that of Ctl hepatocytes (Fig. 3c). In addition, we evaluated gluconeogenesis flux through comparing glucose level in culture medium of hepatocytes from Ctl and OE mice. The glucose-free culture medium contains lactate, pyruvate, and glutamine. After 6 h of culturing, we found that the level of glucose in OE hepatocytes was lower than that of Ctl hepatocytes, which indicated the inhibition of gluconeogenesis in OE mice (Fig. 3d). To further confirm this, gluconeogenesis was enhanced by pCPT-cAMP (a PKA activator). The glucose levels in OE hepatocytes was still lower than that of Ctl hepatocytes (Fig. 3d). Interestingly, most of the SIRT5-regulated proteins in the glycolysis/gluconeogenesis pathway showed significant decrease of malonylation (Fig. 3a and e), whereas the expression level of these proteins remained unchanged (Fig. 3e, gray dot). Collectively, these results suggested that overexpression of SIRT5 enhanced glycolysis and inhibited gluconeogenesis in the hepatocytes of ob/ob mice, probably through demalonylating proteins in this pathway.

To examine whether fatty acid oxidation was affected by overexpressing SIRT5 in liver, we measured the oxygen consumption rate (OCR) of primary hepatocytes from Ctl and OE mice with palmitoylcarnitine used as the substrate. We observed an increase of OCR value in primary hepatocytes from OE mice (Fig. 3h). Similarly, there was a trend of increased succinate oxidation in primary hepatocytes from OE mice, although the increase was not significant (Fig. 3h). Interestingly, there was a significant decrease of succinylation of many proteins in the oxidative phosphorylation pathway (Fig. 3f and g). In the meantime, expression levels of these proteins were relatively unchanged (Fig. 3f, gray dot). In addition, proteins levels of complexes in the oxidative respiratory chain remained comparable between Ctl and OE samples (Fig. 3j). The morphology of mitochondria from the two types of samples was also similar (Fig. 3i). The results indicated that hepatic overexpression of SIRT5 improved mitochondrial fatty acid oxidation of hepatocytes from ob/ob mice by desuccinylating proteins.

3.4. Hepatic overexpression of SIRT5 in ob/ob mice reduces liver TG content

When preparing primary hepatocytes, we observed reduced lipid droplets in OE hepatocytes compared to Ctl under the microscope. To confirm this observation, primary hepatocytes were stained with a lipid droplet probe and observed under a confocal microscope. We discovered that lipid droplets in hepatocytes from OE mice were fewer and smaller than those of Ctl mice (Fig. 4a). In addition, hematoxylin and eosin staining of liver tissue also exhibited a trend of decreased lipid droplets in OE mice (Fig. 4b). To confirm this observation, we isolated the whole liver of each mouse and extracted total lipids via the Soxhlet extractor method using the solvent of diethyl ether. Diethyl ether is a strong solvent for many types of lipids including TG, free fatty acid, sterols, and various phospholipid. However, TG is the main content of lipids in the cell, especially in the liver with steatosis. We found that weight of lipids dropped from an average of 0·92 g (39% of the dehydrated liver) per liver in Ctl mice to 0·68 g (33% of the dehydrated liver) in OE mice (Fig. 4c and d). Furthermore, the weight of dehydrated liver in Ctl mice was 0·3 g heavier (average of 2·3 vs 2·0 g) than that of OE mice (Fig. 4e). Meanwhile, the total body weight and body components remained unchanged (Figs. 4f, S5a and b). Interestingly, we observed slightly elevated level of serum TG in OE mice (Fig. 4g), and similar levels of cholesterol, β-hydroxybutyrate, free fatty acid (FFA), high-density lipoprotein (HDL), and low-density lipoprotein (LDL) (Fig. 4h–j, S5e, and 5f). In addition, indirect calorimetry experiments showed that oxygen consumption (VO_2), respiratory rate (RER = VCO_2 /VO_2), and activity counts remained unchanged (Fig. 4k, l, and S5 h). These results indicated that hepatic overexpression of SIRT5 in ob/ob mice could reduce TG content in liver and attenuated hepatic steatosis.

To investigate glucose metabolism at the whole animal level, we examined the level of blood glucose after hepatic overexpression of SIRT5 and discovered that levels of blood glucose under both fed and fasted conditions were comparable (Fig. S5c and d). To further explore the effect of SIRT5 on regulation of glucose metabolism on the whole animal, the mice were challenged with 2 g glucose/kg body weight injected intraperitoneally and blood glucose was measured at different timepoints. Results demonstrated that there was little improvement of glucose tolerance in OE mice (Fig. S5g). The aforementioned results suggested that hepatic overexpression of SIRT5 has limited effect on the glucose homeostasis at the whole animal level of ob/ob mice.

4. Discussion

In the current study, we generated the ob/ob-SIRT5 OE mice, and observed elevated lactate and ECAR in SIRT5 OE hepatocytes. Considering most of the enzymes in the glycolysis pathway can be regulated by SIRT5, the elevation of lactate and ECAR suggested an improved glycolysis flux. These results are consistent with previous studies by Nishida et al. who showed that SIRT5 regulate glycolysis by demalonylation of related enzymes [18]. However, an alternative explanation for elevation of lactate and ECAR might be the decreased metabolism of glucose-derived pyruvate. Actually, we detected enhanced oxidation of fatty acids after SIRT5 overexpression. Other groups have reported the role of SIRT5 in regulating fatty acid oxidation [17,20]. SIRT5 induced acceleration of fatty acid oxidation pathway might compete with glucose-derived pyruvate oxidation for energy production in the mitochondria. In this case, the elevation of lactate and ECAR could be explained by the inhibition of pyruvate oxidation caused by enhancement of fatty acid oxidation. However, the two explanations are not mutually exclusive. Both mechanisms contribute to the elevation of lactate and ECAR in the OE hepatocytes.

Although we observed increased glucose production in SIRT5 OE hepatocytes, the whole organismal blood glucose levels and glucose tolerance were comparable between Ctl and OE mice. The complicated regulation of glucose metabolism might explain this discrepancy. For example, blood glucose levels are determined by intestinal absorption, hepatic gluconeogenesis, and cellular consumption in muscles. The metabolic improvement in hepatocytes could be overwhelmed by other organs at the whole-animal level. Additionally, the effect of hormones in systemic circulation cannot be ignored. Local levels of insulin and glucagon were capable of reversing some beneficial effects of SIRT5 overexpression.

We also found a decreased hepatic TG content, as well as increased serum TG level in OE mice. However, other lipid metabolites in serum such as FFA, cholesterol, and β-hydroxybutyrate remain comparable in Ctl and OE mice. The ob/ob mice synthesize a huge amount of fatty acid de novo from the carbohydrate in the normal chow diet, and transform them into TG. The hepatic generated TG can either stay in the liver or secrete into serum and be store in adipose tissue. Thus, the decreased hepatic TG content in OE mice might results from decreased de novo synthesis of TG, increased lipolysis and fatty acid oxidation, and enhanced secretion into the circulation system. Our observation suggested that decreased hepatic TG content was caused by increased fatty acid oxidation and enhanced secretion. SIRT5 has been shown to regulate the fatty acid oxidation pathway by many groups. Whether SIRT5 plays an important role in accelerating export of TG from liver to blood remains to be investigated. An interesting cue for this hypothesis is FABPL which has been indicated as an SIRT5 regulated-protein in both SIRT5KO and SIRT5OE data (Fig. S3e and f). FABPL is one of the high-abundance proteins involved in lipid transport in the liver. SIRT5-regulated FABPL might play a role in stimulating hepatic TG secretion.

In addition to the ob/ob-SIRT5 OE mice, we also generated non-ob/ob mice with SIRT5 overexpression (WT-SIRT5 OE). Although there was a significant decrease of malonylation and succinylation in the liver tissue (Fig. S6a), no apparent phenotypes were observed in WT-SIRT5 OE, which is consistent with previous studies of SIRT5 KO mice. In addition, few histopathological changes have been observed (Fig. S6d). Thus, we did not perform the proteomic studies on non-ob/

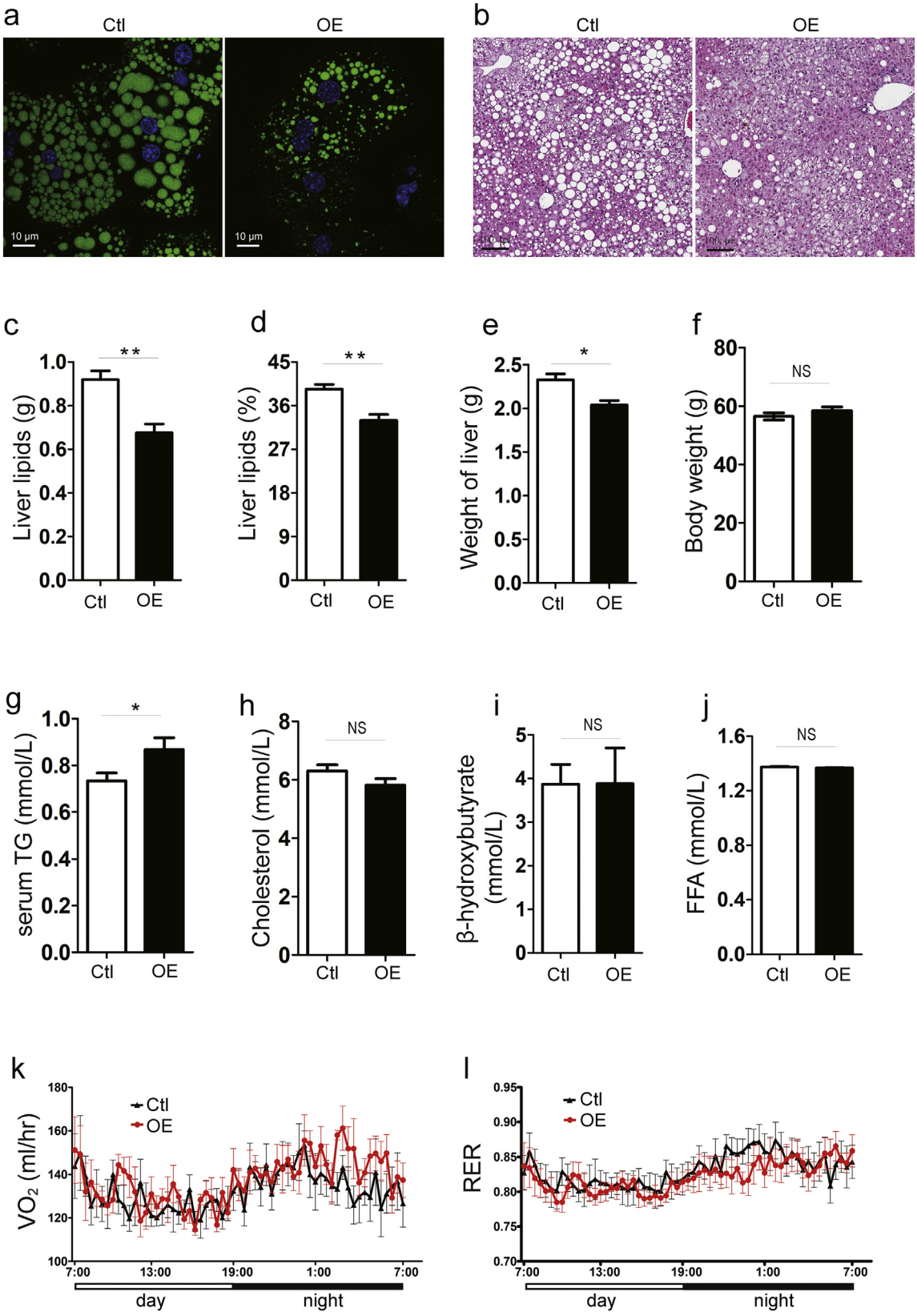

Fig. 4. Hepatic Overexpression of SIRT5 in ob/ob Mice Reduce Liver Triglyceride (TG) Content. (a) Represent image of primary liver cells from Ctl and OE mice. Neutral lipid was stained with probe-Lipid TOX Green. (b) Represent hematoxylin and eosin (H&E) staining of liver tissues from Ctl and OE mice. White dots indicate lipid droplets in cells. (c and d) Liver lipids content of Ctl and OE mice were measured by the Soxhlet extractor method. Lipids were extracted by diethyl ether. The weight loss after diethyl ether extraction represent weight of total lipids in liver (c). The percentage of lipids in liver was calculated as weight of lipids divide by weight of dried liver (d). N = 11–12. (e) Weight of liver tissues from Ctl and OE mice after dried for 7 days. Results are shown as mean ± SE. N = 11–12; *: P < 0·05. (f) Body weight of Ctl and OE mice at the age of 6 month. N = 15–19; NS: non-significant. (g-j) Serum levels of TG (g), Cholesterol (h), β-hydroxybutyrate (i), and FFA (j) of mice. N = 14–18. (k-l) Oxygen consumption and respiratory rate (RER) were detected at different time points for 24 h. N = 8.

ob mice in current study. We analyzed previous malonylome and succinylome data identified in the SIRT5 KO non-ob/ob system. There were 120 SIRT5-regulated malonylated and 140 SIRT5-regulated succinylated proteins identified in the non-ob/ob system [16,18]. Compared with 200 SIRT5-regulated malonylated and 95 SIRT5-regulated succinylated proteins in the ob/ob system, we found 55 and 44 overlapped malonylated and succinylated proteins, respectively (Fig. S6b and c). There were 145 malonylated and 51 succinylated proteins specific regulated in the ob/ob system.

The comparison between the malonylome and succinylome at the level of lysine sites and proteins revealed that these two types of acylation were quite different. The proportion of overlapped proteins that contained at least one malonylation-lysine site and one succinylation-lysine site was <50%. Malonylation proteins localize equally in the cytosol and mitochondria, but succinylation proteins distribute mostly in the mitochondria. The localization pattern is similar to the distribution model of their group donor molecules malonyl-CoA and succinyl-CoA. Malonyl-CoA was first recognized as the intermediate of the fatty acid synthesis pathway and is produced mainly in cytosol by the enzymes acetyl-CoA carboxylases 1 and 2 (ACC1/2). A recent study discovered that malonyl-CoA can also be synthesized directly from malonate by ACSF3 in the mitochondria of mammalian cells [24]. The wide distribution of malonyl-CoA in both the cytosol and mitochondria might explain the malonylated protein localization. In contrast, succinyl-CoA is either mainly synthesized from α-ketoglutarate in the TCA cycle or alternatively synthesized from propionyl-CoA, the β-oxidation products of odd-numbered fatty acids. Both of the synthesizing reactions are in the mitochondria. The exclusive mitochondrial distribution of succinyl-CoA is consistent with the localization of succinylation proteins.

In the present study, we enriched Kmal and Ksucc peptides in the same samples by the sequential immunoprecipitation approach. The disadvantage of the present method is that the first round of enrichment by Kmal antibody might affect the second round of Ksucc enrichment. Although antibodies for each of the acylation are acylation-specific, there might be some cross-reaction of the two antibodies because of the structure similarity of the two types of acylation. We found that the first immunoprecipitation of malonylated peptides induced an approximate 2·5% decrease of the total succinylated peptides identified in the second round of enrichment. Thus, the immunoprecipitation method might slightly affect the comparison between malonylation and succinylation of the same proteins.

Acylation, like malonylation and succinylation, can spontaneously occurs [32], which further indicates that malonylation and succinylation are strongly associated with local concentrations of malonyl-CoA and succinyl-CoA. Metabolic intermediates can locally modify proteins, most of which are metabolic enzymes. The physiological function of these reactions has not yet been elucidated. One explanation is the regulatory role of acylation, which functions as a feedback mechanism to control metabolic flux. The other possibility is the “carbon stress” hypothesis, which is similar to “oxidative stress” [33]. According to the “carbon stress” hypothesis, metabolic intermediates such as malonyl-CoA and succinyl-CoA spontaneously modify proteins and lower the global quality of proteins. In many chronic metabolic diseases such as T2D and cardiovascular diseases, concentrations of intracellular metabolic intermediates are often higher than in healthy individuals. The high concentrations of intermediates modify proteins and disturb their normal functions. Evidence from our current study shows that high levels of sirtuins improve the activity of metabolic pathways, and reverse some abnormal phenotypes probably by lowering the modification of key metabolic enzymes. Our study here provides an alternative method to recognize and understand metabolic abnormality of obesity and T2D which would benefit the therapy of these diseases.

Supplementary data to this article can be found online at https://doi.org/10.1016/j.ebiom.2018.09.037.

Acknowledgments

The authors thank Xiang Ding (Institute of Biophysics, CAS, China) and Mengmeng Zhang (Institute of Biophysics, CAS, China) for assistance with the LC-MS/MS experiment, thank Li Wang (Institute of Biophysics, CAS, China) for assistance with the electron microscope experiment, thank Di liu (Institute of Biophysics, CAS, China) and Jie Zhou (Institute of Biophysics, CAS, China) for assistance with the immunohistochemistry experiment.

Funding sources

This work was supported by the National Key R&D Program of China (2017YFA0205501, 2018YFA0507504), the National Natural Science Foundation of China (31671175, 31771257, 61773025), the Strategic Priority Research Programs (Category A) of the Chinese Academy of Sciences (XDA12030207), the Interdisciplinary Medicine Seed Fund of Peking University (BMU2017MB001) and the National Laboratory of Biomacromolecules.

Declaration of interests

The authors declare no competing interests.

Author contributions

Conceptualization, T.T.W., Y.P.D., and T.T.L.; Methodology, J.F.W., F.Q.Y., T.T.W., and Y.P.D.; Software, S.S.Q. and J.F.W.; Validation, J.F.H., H.H.; Formal Analysis, Y.P.D., S.S.Q., and J.F.W.; Investigation, Y.P.D, H.H., C.J.H., J.L.Z., P.W., and X.L.H.; Writing – Original Draft, Y.P.D.; Writing – Review & Editing, T.T.W. and T.T.L.; Funding Acquisition, T.T.W., T.T.L., and Y.P.D.; Supervision, T.T.W.

References

[1] Haigis MC, Sinclair DA. Mammalian sirtuins: biological insights and disease relevance. Annu Rev Pathol 2010;5:253–95.
[2] Nogueiras R, Habegger KM, Chaudhary N, et al. Sirtuin 1 and sirtuin 3: physiological modulators of metabolism. Physiol Rev 2012;92(3):1479–514.
[3] Gomes P, Outeiro TF, Cavadas C. Emerging role of sirtuin 2 in the regulation of mammalian metabolism. Trends Pharmacol Sci 2015;36(11):756–68.
[4] Anderson KA, Huynh FK, Fisher-Wellman K, et al. SIRT4 is a lysine deacylase that controls leucine metabolism and insulin secretion. Cell Metab 2017;25(4):838–55 [e15].
[5] Liszt G, Ford E, Kurtev M, Guarente L. Mouse Sir2 homolog SIRT6 is a nuclear ADP-ribosyltransferase. J Biol Chem 2005;280(22):21313–20.
[6] Michishita E, McCord RA, Berber E, et al. SIRT6 is a histone H3 lysine 9 deacetylase that modulates telomeric chromatin. Nature 2008;452(7186):492–6.
[7] Tasselli L, Zheng W, Chua KF. SIRT6: Novel Mechanisms and Links to Aging and Disease. Trends Endocrinol Metab 2017;28(3):168–85.
[8] Feldman JL, Baeza J, Denu JM. Activation of the protein deacetylase SIRT6 by long-chain fatty acids and widespread deacylation by mammalian sirtuins. J Biol Chem 2013;288(43):31350–6.
[9] Tong Z, Wang M, Wang Y, et al. SIRT7 is an RNA-activated protein lysine deacylase. ACS Chem Biol 2017;12(1):300–10.
[10] Barber MF, Michishita-Kioi E, Xi Y, et al. SIRT7 links H3K18 deacetylation to maintenance of oncogenic transformation. Nature 2012;487(7405):114–8.
[11] Li L, Shi L, Yang S, et al. SIRT7 is a histone desuccinylase that functionally links to chromatin compaction and genome stability. Nat Commun 2016;7:12235.
[12] Du J, Zhou Y, Su X, et al. Sirt5 is a NAD-dependent protein lysine demalonylase and desuccinylase. Science 2011;334(6057):806–9.
[13] Peng C, Lu Z, Xie Z, et al. The first identification of lysine malonylation substrates and its regulatory enzyme. Mol Cell Proteomics 2011;10(12) M111 012658.
[14] Tan M, Peng C, Anderson KA, et al. Lysine glutarylation is a protein posttranslational modification regulated by SIRT5. Cell Metab 2014;19(4):605–17.
[15] Park J, Chen Y, Tishkoff DX, et al. SIRT5-mediated lysine desuccinylation impacts diverse metabolic pathways. Mol Cell 2013;50(6):919–30.
[16] Rardin MJ, He W, Nishida Y, et al. SIRT5 regulates the mitochondrial lysine succinylome and metabolic networks. Cell Metab 2013;18(6):920–33.
[17] Colak G, Pougovkina O, Dai L, et al. Proteomic and biochemical studies of lysine malonylation suggest its malonic aciduria-associated regulatory role in mitochondrial function and fatty acid oxidation. Mol Cell Proteomics 2015;14(11):3056–71.
[18] Nishida Y, Rardin MJ, Carrico C, et al. SIRT5 regulates both cytosolic and mitochondrial protein malonylation with glycolysis as a major target. Mol Cell 2015;59(2):321–32.

[19] Yu J, Sadhukhan S, Noriega LG, et al. Metabolic characterization of a Sirt5 deficient mouse model. Sci Rep 2013;3:2806.
[20] Sadhukhan S, Liu X, Ryu D, et al. Metabolomics-assisted proteomics identifies succinylation and SIRT5 as important regulators of cardiac function. Proc Natl Acad Sci U S A 2016;113(16):4320–5.
[21] Hershberger KA, Abraham DM, Martin AS, et al. Sirtuin 5 is required for mouse survival in response to cardiac pressure overload. J Biol Chem 2017;292(48):19767–81.
[22] Boylston JA, Sun J, Chen Y, Gucek M, Sack MN, Murphy E. Characterization of the cardiac succinylome and its role in ischemia-reperfusion injury. J Mol Cell Cardiol 2015; 88:73–81.
[23] Du Y, Cai T, Li T, et al. Lysine malonylation is elevated in type 2 diabetic mouse models and enriched in metabolic associated proteins. Mol Cell Proteomics 2015; 14(1):227–36.
[24] Bowman CE, Rodriguez S, Selen Alpergin ES, et al. The mammalian malonyl-CoA synthetase ACSF3 is required for mitochondrial protein malonylation and metabolic efficiency. Cell Chem Biol 2017;24(6):673–84 [e4].
[25] Bandyopadhyay GK, Yu JG, Ofrecio J, Olefsky JM. Increased malonyl-CoA levels in muscle from obese and type 2 diabetic subjects lead to decreased fatty acid oxidation and increased lipogenesis; thiazolidinedione treatment reverses these defects. Diabetes 2006;55(8):2277–85.
[26] Zhao Z, Lee YJ, Kim SK, et al. Rosiglitazone and fenofibrate improve insulin sensitivity of pre-diabetic OLETF rats by reducing malonyl-CoA levels in the liver and skeletal muscle. Life Sci 2009;84(19–20):688–95.
[27] Du Y, Wei T. Inputs and outputs of insulin receptor. Protein Cell 2014;5(3):203–13.
[28] Hippenmeyer S, Youn YH, Moon HM, et al. Genetic mosaic dissection of Lis1 and Ndel1 in neuronal migration. Neuron 2010;68(4):695–709.
[29] Cox B, Emili A. Tissue subcellular fractionation and protein extraction for use in mass-spectrometry-based proteomics. Nat Protoc 2006;1(4):1872–8.
[30] Chen Q, Zhang J, Zhao K, et al. Lysosomal chymotrypsin induces mitochondrial fission in apoptotic cells by proteolytic activation of calcineurin. Protein Cell 2014; 5(8):643–7.
[31] Jiao X, Sherman BT, Huang da W, et al. DAVID-WS: a stateful web service to facilitate gene/protein list analysis. Bioinformatics 2012;28(13):1805–6.
[32] Wagner GR, Payne RM. Widespread and enzyme-independent Nepsilon-acetylation and Nepsilon-succinylation of proteins in the chemical conditions of the mitochondrial matrix. J Biol Chem 2013;288(40):29036–45.
[33] Wagner GR, Hirschey MD. Nonenzymatic protein acylation as a carbon stress regulated by sirtuin deacylases. Mol Cell 2014;54(1):5–16.